Electrically pumped photonic crystal nanocavity light sources using a laterally doped p-i-n junction

Bryan Ellis,[1,a)] Tomas Sarmiento,[2] Marie Mayer,[3] Bingyang Zhang,[1] James Harris,[2] Eugene Haller,[3] and Jelena Vuckovic[1]
[1]*Edward L. Ginzton Laboratory, Stanford, California 94305, USA*
[2]*Department of Electrical Engineering, Stanford University, Stanford, California 94305, USA*
[3]*Materials Sciences Division, Lawrence Berkeley National Laboratory, Berkeley, California 94720, USA and Department of Materials Science, University of California, Berkeley, Berkeley, California 94720, USA*

(Received 25 January 2010; accepted 12 April 2010; published online 4 May 2010)

A technique to electrically pump photonic crystal nanocavities using a lateral p-i-n junction is described. Ion implantation doping is used to form the junction, which under forward bias pumps a gallium arsenide photonic crystal nanocavity with indium arsenide quantum dots. Efficient cavity-coupled electroluminescence is demonstrated and the electrical characteristics of the diode are presented. The fabrication improvements necessary for making an electrically pumped nanocavity laser using a lateral junction are discussed. © *2010 American Institute of Physics*. [doi:10.1063/1.3425663]

Optical interconnects have been proposed as a replacement for electrical interconnects because the loss in electrical wires at high frequencies is becoming a major limitation in information processing devices.[1] To be practical, optical interconnects must therefore consume very little power. For example, one study found that in order for an on-chip optical interconnect to be useful, the entire optical link must consume less than 10 fJ/bit.[2] Semiconductor nanocavity lasers are promising optical sources for this application because they consume little power due to the small active volume and the Purcell effect threshold reduction. The optically pumped photonic crystal (PC) nanocavity laser has been extensively studied because it has been shown to have nanowatt thresholds[3] and high speed modulation rates.[4] In addition, it has been demonstrated that it can operate in continuous wave mode at room temperature,[5] and can be easily integrated with passive elements, such as PC waveguides[6] making them promising for optoelectronic integrated circuits. However, in order for them to be practical, electrical pumping techniques must be developed. In this paper we demonstrate a practical technique to electrically pump a photonic crystal nanocavity and demonstrate efficient cavity coupled electroluminescence (EL). In addition we discuss the fabrication improvements necessary to demonstrate lasing using our technique.

The main challenge of electrically pumping PC membrane nanocavities is how to efficiently inject current into the cavity region. A vertical p-i-n junction in the membrane has been used to electrically pump GaAs PC cavities and to demonstrate reduction of emission rate for cavity coupled EL.[7] However, due to the limited current spreading ability of the thin conductive layers, most of the EL is not coupled to the cavity. A PC nanocavity can be efficiently pumped by using a central current post,[8] and lasing has been demonstrated using this technique. One disadvantage is that the fabrication is complicated, requiring a precisely timed undercut step, and an arbitrary PC design cannot be used since the size and position of the PC holes determine the current post size.[9] In addition, the lasers had a high threshold compared to other electrically pumped microcavity lasers such as micropillars[10] suggesting that the PC lasers suffered from undesirable leakage current.

A lateral p-i-n junction presents a solution to this problem since the current flow can be defined lithographically, and therefore is compatible with arbitrary photonic crystal designs.[11] Ion implantation is a standard method of doping in the electronics industry, and can also be used to dope III-V materials with a lateral junction on a submicron scale. Previous studies of edge-emitting lateral current injection lasers found that the performance was worse than in comparable vertical injection lasers due to a nonuniform carrier distribution in the active region.[12,13] This is because the lasers were fabricated with intrinsic regions wider than the ambipolar diffusion length, which in most III-V materials is approximately 1 μm. Improvements in fabrication techniques should allow the intrinsic region width to be reduced significantly, leading to better performance.

A schematic of the fabrication process is shown in Fig. 1. The wafer used in this experiment consists of a 1 μm $Al_{0.9}Ga_{0.1}As$ sacrificial layer and a 130 nm GaAs membrane with one layer of high density (1×10^{10} cm^{-2}) InAs quantum dots in the middle. First, a dry-etcher is used to define alignment marks. Next Si ions at an energy of 71 keV and a dose of 4×10^{13} cm^{-2} and Mg ions at an energy of 55 keV and a dose of 5×10^{13} cm^{-2} are implanted through a 330 nm nitride mask that is patterned by electron beam lithography. Si and Mg ions are chosen because they offer the best combination of low damage, high activation efficiency, and a low diffusion coefficient. Figure 2(a) shows the ion distribution as a function of depth.[14] The energies of the ions are chosen so that the maximum of the dopant distribution is in the middle of the membrane and the doses are chosen to be well below the amorphization dose. Next, the samples are annealed at 900 °C for 30 s to remove most of the ion implantation induced damage and activate the dopants. It was found that a 30 nm nitride cap was necessary to prevent As outdiffusion during the anneal step. After the anneal, the PC pat-

[a)]Electronic mail: bryane@stanford.edu.

 © 2010 American Institute of Physics

Downloaded 04 May 2010 to 171.64.85.131. Redistribution subject to AIP license or copyright; see http://apl.aip.org/apl/copyright.jsp

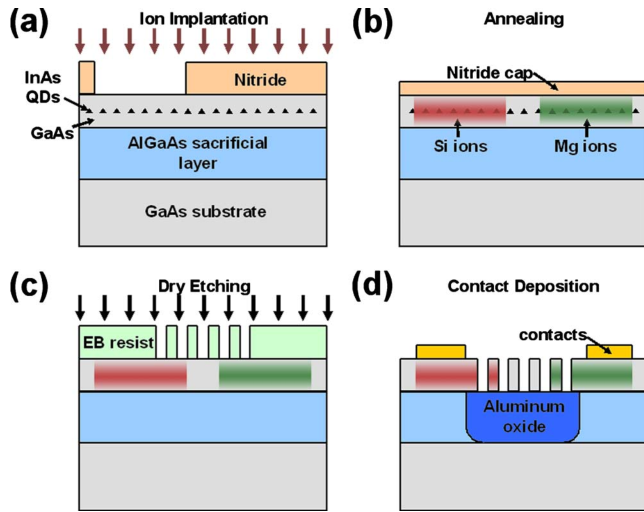

FIG. 1. (Color online) Schematic illustration of fabrication process (a) Si and Mg ions are implanted through a silicon nitride mask patterned by electron beam lithography (b) The implanted dopants are activated by annealing at 900 °C for 30 s with a nitride cap which is subsequently removed by dry etching. (c) The photonic crystal pattern is defined in a resist by electron beam lithography and transferred into the GaAs membrane by dry etching (d) The $Al_{0.9}Ga_{0.1}As$ sacrificial layer is oxidized and the p and n contacts are deposited by photolithography and liftoff.

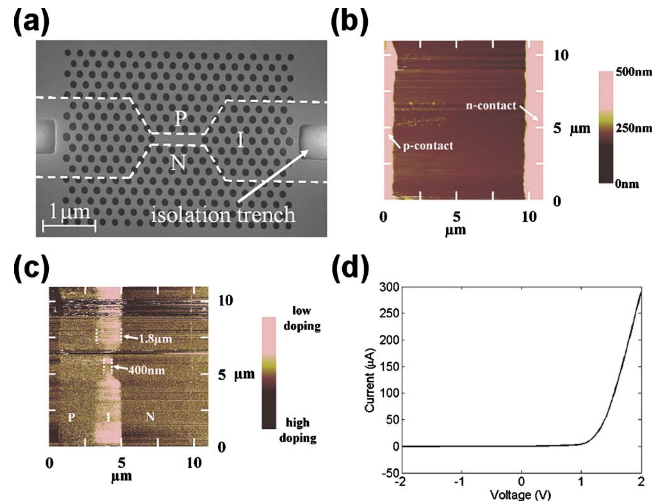

FIG. 3. (Color online) (a) Scanning electron microscope image of PC nanocavity. The isolation trenches beside the cavity confine current to the cavity region. The edges of the p and n doped regions are indicated by the white dashed lines. [(b) and (c)] Scanning capacitance microscope images of doping distribution before PC fabrication showing topography (b) and corresponding dC/dV amplitude (c). The p-region is on the left side of the image, and the n-region is on the right. (d) *IV* curve of ten photonic crystal cavities electrically connected in parallel.

terns were defined by electron beam lithography and dry-etched into the membrane. The $Al_{0.9}Ga_{0.1}As$ sacrificial layer underneath the GaAs membrane was then oxidized in an oxidation furnace. Next a Au–Ge–Ni–Au n-type contact and a Au–Zn–Au p-type contact were deposited, and the contacts were annealed at 450 °C for one minute. Based on the results of Hall effect and electrochemical capacitance voltage measurements we estimate the maximum n-type doping concentration in the middle of the membrane to be about 8×10^{17} cm^{-3} and the maximum p-type doping concentration to be about 3×10^{18} cm^{-3}. These concentrations are consistent with dopant activation efficiencies measured elsewhere.[15]

To study the effect of the doping process on the quantum dot photoluminescence (PL), the samples were cooled to 30 K. The cooling is necessary because the shallow-confinement InAs quantum dots do not emit at room temperature. Figure 2(b) shows the quantum dot PL from a region with no implanted ions before and after the activation anneal. The quantum dot density in our wafer is too high to see the emission lines of individual quantum dots, and we instead see a Gaussian distribution of emission where the full-width half maximum (FWHM) is determined by the inhomogeneous broadening of the dot ensemble. The quantum dot emission is grown to be centered at 940 nm; however the activation anneal step causes the dots to blueshift by about 30 nm. Interestingly, the FWHM of the quantum dot emission is reduced by a factor of 2, indicating a reduction of the inhomogeneous broadening. Previous studies of this effect have found that rapid thermal annealing of quantum dots can actually be beneficial for laser applications because the FWHM of the dot distribution narrows, increasing the available gain;[16] however the blueshift of the emission wavelength must be compensated for during the growth. Ion implantation induced damage introduces nonradiative recombination centers, and the PL intensity was observed to decrease significantly in the implanted regions, similar to what has been observed in other experiments.[12,13] The unimplanted regions are left undamaged, so the emission intensity there is unaffected.

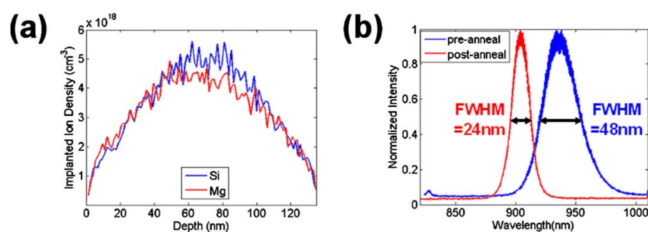

FIG. 2. (Color online) (a) Simulated density of implanted ions as a function of depth (b) Normalized PL intensity of quantum dots before and after the activation anneal showing the reduction in FWHM.

The doping layout is shown in Fig. 3(a). We employ a linear, three hole defect PC cavity design where the end holes have been shifted to increase the quality factor.[17,18] Away from the cavity region the intrinsic region is wider than the ambipolar diffusion length. The combination of the wide intrinsic region of the diode and the PC holes form a high resistance region reducing leakage current. In the cavity region the intrinsic region of the diode is designed to be between 200 and 400 nm wide. To confirm that dopant diffusion during the activation anneal does not drastically change the dopant layout, a scanning capacitance atomic force microscope was used to image the dopant distribution on devices without PCs. Figure 3(b) shows the topography image of the device, and Fig. 3(c) shows the change in capacitance with applied voltage (dC/dV) amplitude image. Together these indicate the presence of the desired doping without topographical effects. To make the cavities easier to test electrically, the cavities were electrically connected in parallel, ten of them per pair of contacts. The current-voltage (*IV*) curve of ten cavities in parallel is shown in Fig. 3(d). From this we infer that the current density in the cavity region is high, around 10^3 A/cm^2 at an applied voltage of 1.5 V. Previous studies of the electrical properties of doped photonic crystals have found that the surface depletion region

Downloaded 04 May 2010 to 171.64.85.131. Redistribution subject to AIP license or copyright; see http://apl.aip.org/apl/copyright.jsp

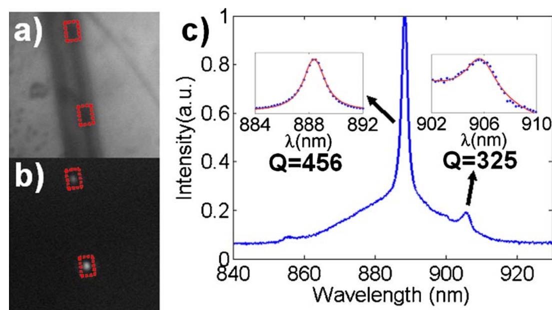

FIG. 4. (Color online) [(a) and (b)] Microscope image of photonic crystal cavities (a) and corresponding image of the EL at 1.6 V (b). The locations of the two cavities are outlined with red dashed lines. The p-contact is on the right and the n-contact on the left. (c) EL spectrum of the cavity on the top of (b). The insets show Lorentzian fits (solid lines) to the experimental cavity spectrum (data points) to determine the quality factor.

around the holes affects the series resistance.[19] This is because the depletion region at the hole edges, and at the top and bottom of the membrane decreases the available volume for conduction. Carrier transport in the photonic crystal is determined by the electrical effective air fill factor $f_{\mathrm{elec}} = (\pi/2\sqrt{3})[(d+2\delta)^2/a^2]$ where δ is the depletion width, d is the membrane thickness, and a is the spacing between photonic crystal holes.[19] We estimate that the depletion width δ is approximately 45 nm and 30 nm in the n- and p-type regions, respectively, indicating that the membrane is likely not fully depleted.

Next, the sample was cooled to 30 K, 1.6 V of forward bias was applied to the cavity, and the EL was imaged by a confocal microscope. Figure 4(a) shows the microscope image of the cavities under white light illumination, and Fig. 4(b) shows the corresponding image of the EL. The EL is confined to the cavity region, confirming that the devices have a low leakage current. A pinhole is used to collect the emission from only one cavity, and the spectrum of a single cavity is shown in Fig. 4(c). Two cavity modes are observed with quality factors of approximately 400. Finite-difference time-domain (FDTD) simulations indicate that the highest wavelength mode is the fundamental mode of the cavity. The simulated Q of the cavity is approximately 2000, and is limited by the high refractive index ($n \approx 1.72$) aluminum oxide layer under the cavity. No lasing was observed from the cavities even at high current and pulsed pumping conditions. However, we point out that the demonstrated structures are also interesting for a variety of electrically injected devices in addition to lasers such as light–emitting devices (LEDs) and modulators that do not require gain.

We now consider the limitations of the current device which prevent it from reaching the lasing regime. Lasing from photonic crystal nanocavities has been previously demonstrated with optical pumping in this material.[18] The condition for optical gain is the Bernard–Duraffourg condition, $(F_c - F_v) > \hbar\omega$ (Ref. 20) where $(F_c - F_v)$ is the separation of the quasi-Fermi levels and $\hbar\omega$ is the emission energy. From Poisson simulations, we conclude that the doping densities in our device are not high enough to satisfy this condition. This indicates that the doping must be increased to reach population inversion and lasing. Simulations of the ion implantation induced damage indicate that the ion doses for both the Si and Mg doping steps can be increased by about a factor of 5 before the damage begins to amorphize the membrane. Because some of this damage will be annealed out in the activation step, it is not clear how much the ion dose can be increased before there is too much damage to achieve lasing. Alternatively a lighter dopant such as Be will generate fewer vacancies during implantation, and therefore can be used to achieve higher doping densities. Be has been used to demonstrate ion implantation doped edge emitting lasers in GaAs before.[13]

In summary, we have demonstrated that a lateral p-i-n junction can be used to electrically pump a GaAs PC nanocavity. The properties of an ion implantation doped PC LED are studied, and efficient EL from an L3 nanocavity is demonstrated. The electrical properties of the device and the improvements necessary to make a laser are presented.

The authors would like to acknowledge Peter Stone and Jeff Beeman for help with ion implantation, and Professor Yoshihisa Yamamoto for help with sample growth. Financial support for this work was provided by the Gould Foundation, the Stanford Graduate Fellowship, and the NDSEG Fellowship. The authors acknowledge the support of the Interconnect Focus Center, one of six research centers funded under the Focus Center Research Program (FCRP), a Semiconductor Research Corporation entity. Financial assistance for B.Y.Z. was provided in part by JST/SORST.

[1]D. Miller, Proc. IEEE **88**, 728 (2000).
[2]D. Miller, Proc. IEEE **97**, 1166 (2009).
[3]S. Strauf, K. Hennessy, M. Rakher, Y. Choi, A. Badolato, L. Andreani, E. Hu, P. Petroff, and D. Bouwmeester, Phys. Rev. Lett. **96**, 127404 (2006).
[4]H. Altug, D. Englund, and J. Vuckovic, Nat. Phys. **2**, 484 (2006).
[5]M. Nomura, S. Iwamoto, K. Watanabe, N. Kumagai, Y. Nakata, S. Ishida, and Y. Arakawa, Opt. Express **14**, 6308 (2006).
[6]K. Nozaki, H. Watanabe, and T. Baba, Appl. Phys. Lett. **92**, 021108 (2008).
[7]M. Francardi, L. Balet, A. Gerardino, N. Chauvin, D. Bitauld, L. H. Li, B. Alloing, and A. Fiore, Appl. Phys. Lett. **93**, 143102 (2008).
[8]H. Park, S. Kim, S. Kwon, Y. Ju, J. Yang, J. Baek, S. Kim, and Y. Lee, Science **305**, 1444 (2004).
[9]H.-G. Park, S. Kim, M. Seo, Y. Ju, S. Kim, and Y. Lee, IEEE J. Quantum Electron. **41**, 1131 (2005).
[10]S. Reitzenstein, T. Heindel, C. Kistner, A. Rahimi-Iman, C. Schneider, S. Hofling, and A. Forchel, Appl. Phys. Lett. **93**, 061104 (2008).
[11]C. Long, A. Giannopoulos, and K. Choquette, Electron. Lett. **45**, 227 (2009).
[12]E. Sargent, G. Tan, and J. Xu, IEEE J. Sel. Top. Quantum Electron. **3**, 507 (1997).
[13]A. Tager, R. Gaska, I. Avrutzky, M. Fay, H. Chik A. SpringThorpe, S. Eicher, J. Xu, and M. Shur, IEEE J. Sel. Top. Quantum Electron. **5**, 664 (1999).
[14]J. Ziegler, M. Ziegler, and J. Biersach, SRIM—The Stopping and Range of Ions in Matter, Version 2008.03, www.srim.org (2008).
[15]P. Pronko, Y. Yeo, R. Bhattacharya, and A. Rai, *Ion Implantation in III-V Compound Semiconductors*, Air Force Wright Aeronautical Laboratories Report No. AD-A148 462, 1984 (http://www.scientificcommons.org/19837891).
[16]S. Malik, C. Roberts, R. Murray, and M. Pate, Appl. Phys. Lett. **71**, 1987 (1997).
[17]Y. Akahane, T. Asano, B. Song, and S. Noda, Nature (London) **425**, 944 (2003).
[18]B. Ellis, I. Fushman, D. Englund, B. Zhang, Y. Yamamoto, and J. Vuckovic, Appl. Phys. Lett. **90**, 151102 (2007).
[19]A. Berrier, M. Mulot, G. Malm, M. Ostling, and S. Anand, J. Appl. Phys. **101**, 123101 (2007).
[20]M. Bernard and G. Duraffourg, Phys. Status Solidi **1**, 699 (1961).

Downloaded 04 May 2010 to 171.64.85.131. Redistribution subject to AIP license or copyright; see http://apl.aip.org/apl/copyright.jsp